# Microporous Battery Electrodes from Molecular Cluster Precursors

Alexander P. Aydt,[†,∥] Boyu Qie,[‡,∥] Andrew Pinkard,[†,∥] Long Yang,[‡] Qian Cheng,[‡]
Simon J. L. Billinge,[‡,§] Yuan Yang,[*,‡] and Xavier Roy[*,†]

[†]Department of Chemistry and [‡]Program of Materials Science and Engineering, Department of Applied Physics and Applied Mathematics, Columbia University, New York, New York 10027, United States

[§]Condensed Matter Physics and Materials Science Department, Brookhaven National Laboratory, Upton, New York 11973, United States

S *Supporting Information*
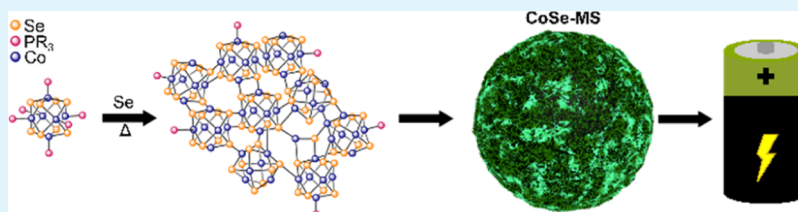
ABSTRACT: Developing novel energy storage materials is critical to many renewable energy technologies. In this work, we report on the synthesis and electrochemical properties of materials composed of porous cobalt selenide microspheres prepared from molecular cluster precursors. The cobalt selenide microspheres excel as Na^+ ion battery electrode materials, with a specific capacity of ~550 mA h/g and excellent cycling stability of 85% over 100 cycles, and perform equally well as Li^+ ion battery electrodes with a specific capacity of ~600 mA h/g and cycling stability of 80% over 100 cycles. Materials which reversibly store large amounts of Na^+ ions are uncommon, and these performances represent significant advances in the field. More broadly, this work establishes metal chalcogenide molecular clusters as valuable precursors for creating new, tunable energy storage materials.

KEYWORDS: *cluster compounds, microspheres, electrochemistry, batteries, conducting material*

Cobalt chalcogenides have attracted considerable attention because of their rich structural chemistry and their potential use in hydrodesulfurization,[1,2] electrocatalysis,[3,4] dye-sensitized solar cells,[5,6] supercapacitors,[7−9] and battery[10−14] applications. While a variety of cobalt chalcogenide polymorphs can be prepared using bulk syntheses (e.g., solid state,[15] solution phase,[13] and solvothermal reactions[16]), there is a sustained interest in creating nanostructures whose performances can surpass their bulk crystalline counterparts because of unique structures, morphologies, quantum confinement effects, and surface properties.[17,18]

Here, we report a new material composed of microporous cobalt chalcogenide microparticles synthesized from molecular cluster precursors and their performances as battery electrode materials. Recently deployed as superatomic building blocks to create functional materials,[19,20] metal chalcogenide molecular clusters have previously been shown to convert to bulk crystalline solids by removing their passivating ligands via thermolysis.[21,22] Other well-defined clusters have been used as electronic or catalytic dopants in hybrid materials.[23−25] In this work, we develop a new solution-phase chemical approach to dissociate the capping ligands from the molecular cluster $Co_6Se_8(PEt_3)_6$ using elemental Se as a phosphine scavenger. The resulting cobalt selenide microspheres, designated as **CoSe-MS**, have high surface areas and robust electrochemical properties, a combination that is particularly attractive for battery applications. We find that the material performs best

for Na^+ ion battery applications relative to similar materials, with a high specific capacity (~550 mA h/g) and excellent cycling performances (85% retention after 100 cycles). Likewise, **CoSe-MS** functions well as anode materials for Li^+ ions (~600 mA h/g and cycling stability of 80% over 100 cycles).

Figure 1 illustrates the synthesis of **CoSe-MS**, starting from the parent molecular cluster $Co_6Se_8(PEt_3)_6$. The synthesis of these cluster precursors from $Co_2(CO)_8$, PEt_3, and Se is detailed in the Supporting Information.[22] To dissociate PEt_3 from the Co_6Se_8 core, we combine the molecular cluster with six equivalents of Se in toluene and heat the suspension to 150 °C in a thick wall vessel sealed under N_2 with a Teflon stopper. A black solid, **CoSe-MS**, precipitates after 24 h and is collected under a N_2 atmosphere by filtration and dried in vacuo. The key concept is that the phosphine ligands are somewhat labile at high temperatures in solution and upon dissociation from the core, they become kinetically trapped as $Et_3P\!\!=\!\!Se$. We propose that upon ligand dissociation, the naked cluster cores first fuse together through Co—Se linkages to form an extended structure. Champsaur et al. recently reported a related fusion reaction in a model Co_6Se_8 cluster.[26]
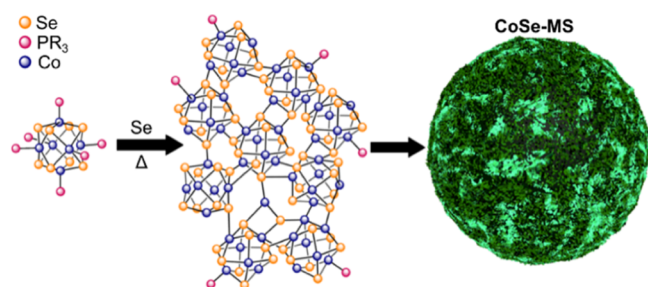
Figure 1. Schematic illustrating cluster-based synthesis of **CoSe-MS**. Elemental Se acts as a phosphine scavenger allowing for cluster cores to bridge via Co−Se linkages. The resulting materials are highly porous

Scanning electron microscopy (SEM) reveals that **CoSe-MS** consists of microscopic spheres of cobalt selenide with diameters typically in the range 0.5−1 μm (Figure 2). The high-magnification SEM images of the microspheres shown in Figure 2a,b hint at a porous structure. N_2 adsorption isotherm measurements and Brunauer−Emmett−Teller analysis confirm this key observation: the N_2 isotherms for **CoSe-MS** in Figure S4 show H4-type hysteresis loops associated with microporous or mesoporous structures.[27] **CoSe-MS** has a specific surface area of ~130 m^2/g and an average pore diameter of ~1.7 nm, as estimated by Barrett−Joyner−Halenda analysis (Table S2).

X-ray pair distribution function (PDF) analysis[28] is performed on **CoSe-MS** to further investigate its structure. A strategy of testing all the structures composed of Co and Se, available at the Inorganic Crystal Structure Database, (ICSD)[29] is used. The best fit is obtained for a nanocrystalline Co_3Se_4 (NC-Co_3Se_4) structure model (Figure 2c inset).[30] Closer inspection of the fit in Figure 2c suggests that this model fits the PDF peaks well in the high-r region, but additional unfit signal is evident in the difference curve in the low-r region. We, therefore, explore a two-phase model where a second structure is added to the NC-Co_3Se_4 model but given a

much shorter range of structural coherence to explain the extra signal in the low-r region. The best agreement was obtained by adding a second NC-Co_3Se_4 phase with a small spherical particle diameter. The resulting PDF fit of short range-ordered (SRO) NC-Co_3Se_4 + longer range-ordered (LRO) NC-Co_3Se_4 model, with a goodness of fit parameter, $R_w = 0.159$, is shown in Figure 2d. The refined structural parameters are shown in Table S3. The fit is greatly improved over the single-phase fit. The detailed structural modeling and the method for PDF measurements[28,31−40] can be found in the Supporting Information.

In agreement with the PDF results, the powder X-ray diffraction pattern of **CoSe-MS** matches that of Co_3Se_4 (Figure S1). Energy-dispersive X-ray (EDX) spectroscopy establishes the composition of the solid as $CoSe_{1.2}P_{0.1}$ (Table S1), suggesting ~10% Se deficiency in the material.

With a porous structure and spherical morphology, **CoSe-MS** differs significantly from other cobalt chalcogenide materials. To illustrate this, we annealed **CoSe-MS** at 400 °C for 4 h (**CoSe-1**, Table 1). The microsphere morphology is maintained (Figure S2) but the internal surface area of **CoSe-1** is dramatically decreased to 7 m^2/g. The N_2 isotherms show essentially no hysteresis, consistent with a nonporous structure. The final composition of **CoSe-1** is $CoSe_{1.1}P_{0.01}$ as determined by EDX. Note that the annealed compounds show a loss of crystallinity (Figure S1). We also prepared an additional comparison material by sealing pristine microcrystalline $Co_6Se_8(PEt_3)_6$ in a quartz tube and heating the material to 400 °C to dissociate PEt_3 (**CoSe-2**, Table 1). The SEM images of the resulting materials reveal that this approach produces submicron irregular particles (Figure S2) that differ drastically from **CoSe-MS**.

The combination of the microspherical morphology, microporosity, and crystalline structure imparts **CoSe-MS** with unique electrochemical properties. To explore these properties, we fabricated working electrodes by depositing a slurry of the material, carbon black, and polyvinylidenefluoride onto Cu
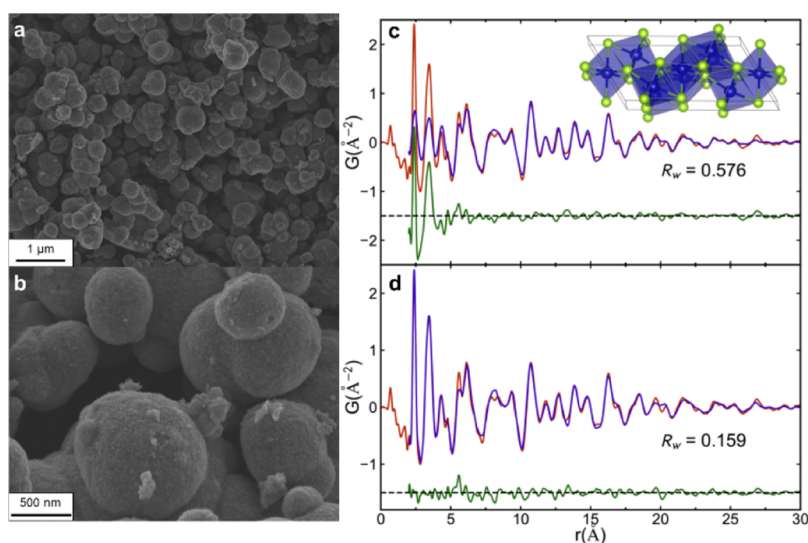
Figure 2. (a,b) SEM images of **CoSe-MS** at (a) low magnification and (b) high magnification. (c,d) X-ray PDF of the **CoSe-MS** data (red curve) with (c) the best-fit calculated PDF (purple) for the NC-Co_3Se_4 model. The model was fit over a region of 5 < r < 30 Å, but the plot shows the calculated curve extended to low-r. (d) Best-fit calculated PDF (purple) for the two-phase SRO NC-Co_3Se_4 + LRO NC-Co_3Se_4 model. The fit was done over a range of 2 < r < 30 Å. The difference curves are shown offset below (green). The inset in (c) is the NC-Co_3Se_4 structure, where Co atoms are in blue and Se atoms are in green.

Table 1. Synthesis, Specific Surface Areas, and Electrochemical Performances of CoSe-MS and Control Materials

name	synthesis	initial capacity (mA h/g)	cycles/capacity retention	specific surface area (m²/g)
CoSe-MS/Li	$Co_6Se_8(PEt_3)_6$ and Se in toluene at 150 °C	602	100/80%	131
CoSe-1/Li	**CoSe-MS** annealed at 400 °C	442	100/35%	7
CoSe-MS/Na	$Co_6Se_8(PEt_3)_6$ and Se in toluene at 150 °C	554	100/85%	131
CoSe-1/Na	**CoSe-MS** annealed at 400 °C	520	100/5%	7
CoSe-2/Na	thermolysis of $Co_6Se_8(PEt_3)_6$ at 400 °C	470	75/50%	NA
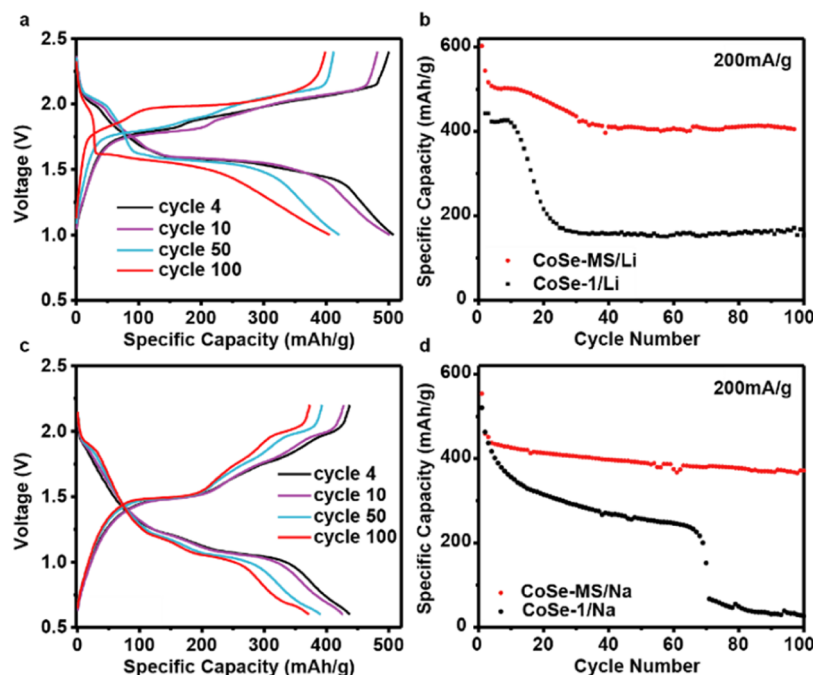
Figure 3. (a) Galvanostatic charge and discharge profiles of **CoSe-MS** vs Li/Li⁺ in 1 M LiTFSI (TFSI = bis(trifluoromethanesulfonyl)imide) in dioxolane (DOL) at 50 mA/g for the first three cycles, followed by 200 mA/g for the rest of the experiment. (b) Cycle stability of **CoSe-MS**/Li and **CoSe-1**/Li half-cells. The testing conditions are the same as in (a). (c) Galvanostatic charge and discharge profiles of **CoSe-MS** vs Na/Na⁺ in 1 M NaPF₆ in 1:1 DOL/DME (DME = dimethoxyethane) at 50 mA/g for the first two cycles, followed by 200 mA/g for the rest of the experiment. (d) Cycle stability of **CoSe-MS**/Na and **CoSe-1**/Na half-cells. The testing conditions are the same as in (c).

substrates. All electrochemical analyses are performed in coin cells with the Li or Na metal as the counter electrode (details of the working electrode, electrolytes, and cell fabrication are in the Supporting Information). We find that **CoSe-MS** works best as Na⁺ ion battery electrode materials, although it is an adequate Li⁺ ion battery electrode material. Highlighting these findings, Figure 3 presents the galvanostatic voltage data of **CoSe-MS** on both ions.

At a current density of 50 mA/g, the **CoSe-MS**/Li cell shows an initial capacity of 602 mA h/g. When the current density is increased to 200 mA/g after two cycles, the initial capacity is 507 mA h/g; it remains at ~405 mA h/g after 100 cycles at 200 mA/g, for a capacity retention of 80% (Figure 3a). While the exact reason for this capacity loss remains unclear, we note that it is mainly due to the shortening of the plateau at 1.5 V. One likely cause is the conversion reaction between the material and Li⁺ ions. SEM confirms that the morphology of the electrode material is essentially unchanged after cycling (Figure S3), indicating that the microporous structure allows the structure to release the strains created by the conversion reaction and prevents the spherical particles from breaking apart, leading to reasonable cycling. Based on the voltage profile and specific capacity, we infer that the overall electrochemical reaction is $Co_3Se_4 + 8Li \rightarrow 3Co + 4Li_2Se$

for Co_3Se_4/Li cells and $Co_3Se_4 + 8Na \rightarrow 3Co + 4Na_2Se$ for Co_3Se_4/Na cells.[18]

To gain further insight into the electrochemical properties of **CoSe-MS**, we performed galvanostatic cycling experiments and compared the performances of these nanomaterials with those of the annealed control samples (Figures 3b and S7). Overall, these measurements confirm the higher capacity and significantly better cycling stability of the microporous **CoSe-MS**. When comparing **CoSe-MS** with nonporous **CoSe-1**, we observe vastly different behaviors: the initial capacity is lower (442 mA h/g at current density 50 mA/g) and decays faster to 156 mA h/g after 100 cycles. This represents a capacity retention of only 35%. Moreover, electrochemical impedance spectroscopy (EIS) measurements of **CoSe-MS**/Li and **CoSe-1**/Li cells suggest that the microporous structure of **CoSe-MS** provides better diffusion kinetics for different charge states, when compared to a nonporous material (Figure S8).

Remarkably, **CoSe-MS** excels for Na⁺ ions. The design of high-performance anode materials for Na⁺ ion batteries is more challenging than Li⁺ ion batteries because of the sluggish solid-state diffusion of Na⁺.[41] Traditional compounds such as metal oxides, metal chalcogenides, and carbonaceous materials suffer from low specific capacities (200−300 mA h/g) at higher current densities and restricted cycle life due to high volume expansion.[42−45] As a reference, state-of-the-art chalcogenide-
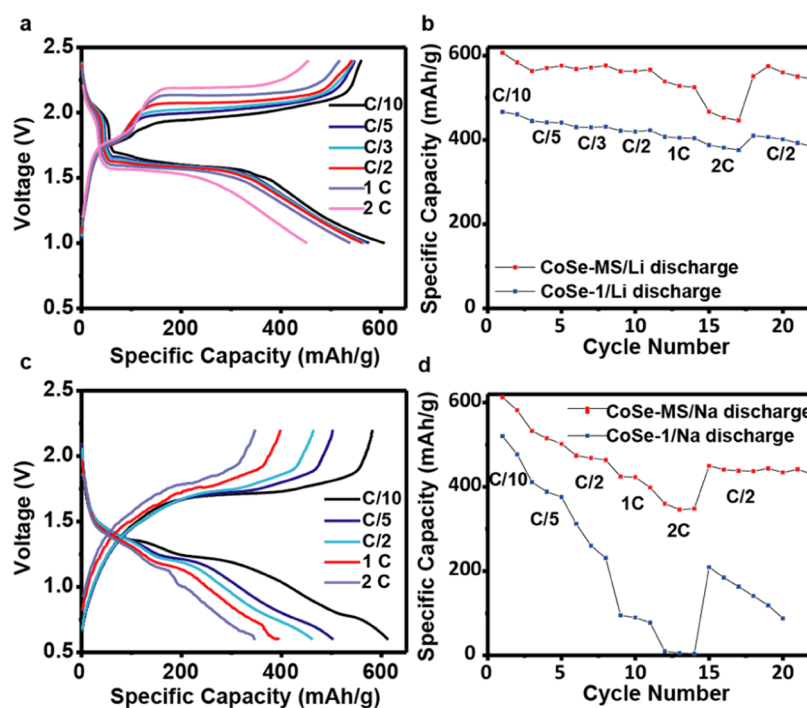
Figure 4. (a) Representative charge and discharge profiles of **CoSe-MS**/Li half-cells at various rates from 0.1 to 2 C. (b) Rate capacity of the **CoSe-MS**/Li half-cells at various rates from 0.1 to 2 C (1 C = 500 mA/g). (c) Representative charge and discharge profiles of **CoSe-MS**/Na half-cells at various rates from 0.1 to 2 C. (d) Rate capacity of the **CoSe-MS**/Na and **CoSe-1**/Na half-cells at various rates from 0.1 to 2 C (1 C = 500 mA/g).

based Na^+ ion battery materials such as MoS_2 nanoflowers, Cu-doped $CoSe_2$ microboxes, and hollow $CoSe_2$ microspheres show specific capacities of 350 mA h/g after 300 cycles,[46] 400 mA h/g after 500 cycles,[47] and 467 mA h/g after only 40 cycles,[18] respectively.

In this context, the electrochemical properties of the **CoSe-MS**/Na cell presented in Figure 3c,d are exciting. The cyclic voltammogram (CV) reveals that the main cathodic and anodic peaks, respectively, at 1.0 and 1.5 V versus Na^+/Na, are essentially unchanged after cycling, indicating a reversible reaction (Figure S6) likely similar to other described mechanisms.[18] A new peak at 0.6 V versus Na^+/Na, which gradually grows in with each cycle, suggests that the structure of the material is changing, potentially forming polyselenides.

The galvanostatic voltage profile of **CoSe-MS**/Na measured at a current density of 200 mA/g reflects the features in voltammogram (Figure 3c). During discharge, after a short plateau at 1.8 V, the voltage quickly drops down to 1.2 V, at which point a second, longer plateau occurs between 1.2 and 1 V. This plateau corresponds to the major peak at 1.0 V in the CV. Upon cycling, an additional plateau gradually appears at 0.7 V, which is consistent with the peak growing at 0.6 V in the CV.

To evaluate performance in battery applications, the **CoSe-MS**/Na cell is initially cycled at a current density of 50 mA/g for three cycles: the initial capacity is 554 mA h/g (Figures 3d and S7). The current density is then increased to 200 mA/g for 100 cycles: the capacity starts at 437 mA h/g and decreases to 371 mA h/g at the 100th cycle, for a capacity retention of 85%. By comparison, **CoSe-1**/Na has lower initial capacities of 520 and 417 mA h/g at current densities of 50 and 200 mA/g, respectively. The capacity decreases to 60 mA h/g after only 70 cycles. Also, **CoSe-2** has an initial capacity of 470 mA h/g at 200 mA/g but only has a capacity retention of 50% after 75

cycles (Figure S7). The capacity is also much better than previous reports on transition-metal selenides.[48] These results indicate that the microporous structure of **CoSe-MS** is critical in determining the electrochemical performance of the material, presumably by enabling transport of the Na^+ ions and reducing the lattice strains. This is supported by SEM images of the **CoSe-MS** electrode after 100 cycles, showing intact microspheres. EIS data of **CoSe-MS**/Na and **CoSe-1**/Na cells (Figure S8) also strongly imply that the microporous structure of **CoSe-MS** significantly enhances the diffusion kinetics of Na^+ ions.

The microporosity also improves the power capacity of the materials as ions can access higher surface areas and the diffusion through the solid is reduced. The **CoSe-MS**/Li cell delivers capacities of 576, 568, 563, 539, and 467 mA h/g at rates of 0.2, 0.33, 0.5, 1, and 2 C (1 C = 500 mA/g), respectively, which are 95, 94, 93, 89, and 77% of that at 0.1 C (606 mA h/g) (Figure 4). The plateaus at 1.5 V are unchanged, indicating that the reaction mechanism remains the same across different current densities (Figure 4a). Similarly, the **CoSe-MS**/Na cell shows attractive performance across a wide range of rates, even though the Na^+ ions are much larger than Li^+ ions. The cell delivers capacities of 532, 474, 424, and 360 mA h/g at rates of 0.2, 0.5, 1, and 2 C, respectively, corresponding to 87, 77, 69, and 59% of that at 0.1 C (612 mA h/g) (Figure 4b), with the same shape of voltage profiles. When compared to nonporous control material **CoSe-1**, the power capacity and cycling stability of **CoSe-MS** are much better (Figure 4b,d). These results show that the high surface area and microporosity of **CoSe-MS** can improve the reaction and ion-diffusion kinetics, enabling excellent power capacities.

In summary, we have developed a mild chemical approach to convert cobalt selenide molecular clusters into polycrystalline

mesoporous microspheres. Because of their porosities, high surface areas, and robust electrochemical properties, these new materials exhibit excellent performances in Li^+ and Na^+ ion battery electrode applications. These results chart a clear path to expand the development of energy storage materials using molecular cluster precursors.

■ ASSOCIATED CONTENT

ⓢ Supporting Information

The Supporting Information is available free of charge on the ACS Publications website at DOI: 10.1021/acsami.8b18149.

> Experimental procedures, battery fabrication methods, instrumentation details, and supplementary figures and tables are given via a link at the end of the document (PDF)

■ AUTHOR INFORMATION

Corresponding Authors

*E-mail: yy2664@columbia.edu (Y.Y.).
*E-mail: xr2114@columbia.edu (X.R.).

ORCID Ⓘ

Long Yang: 0000-0001-8731-0172
Qian Cheng: 0000-0001-5510-2977
Simon J. L. Billinge: 0000-0002-9734-4998
Yuan Yang: 0000-0003-0264-2640
Xavier Roy: 0000-0002-8850-0725

Author Contributions

∥A.P.A., B.Q., and A.P. contributed equally to this work.

Notes

The authors declare no competing financial interest.

■ REFERENCES

(1) Delmon, B.; Grange, P. The Role of Cobalt and Molybdenum Sulphides in Hydrodesulphurisation Catalysts: A review. *J. Less Common Met.* **1974**, *1*, 353−360.

(2) Bouwens, S. M. A. M.; Van Veen, J. A. R.; Koningsberger, D. C.; De Beer, V. H. J.; Prins, R. EXAFS Determination of the Structure of Cobalt in Carbon-supported Cobalt and Cobalt-molybdenum Sulfide Hydrodesulfurization Catalysts. *J. Phys. Chem.* **1991**, *95*, 123−134.

(3) Sun, Y.; Liu, C.; Grauer, D. C.; Yano, J.; Long, J. R.; Yang, P.; Chang, J. S. Electrodeposited Cobalt-Sulfide Catalyst for Electro-chemical and Photoelectrochemical Hydrogen Generation from Water. *J. Am. Chem. Soc.* **2013**, *135*, 17699−17702.

(4) Bonde, J.; Moses, P. G.; Jaramillo, T. F.; Nørskov, J. K.; Chorkendorff, I. Hydrogen Evolution on Nano-Particulate Transition Metal Sulfides. *Faraday Discuss.* **2009**, *140*, 219−231.

(5) Wang, M.; Anghel, A. M.; Marsan, B.; Cevey Ha, N.-L.; Pootrakulchote, N.; Zakeeruddin, S. M.; Grätzel, M. CoS Supersedes Pt as Efficient Electrocatalyst for Triiodide Reduction in Dye-Sensitized Solar Cells. *J. Am. Chem. Soc.* **2009**, *131*, 15976−15977.

(6) Kung, C.-W.; Chen, H.-W.; Lin, C.-Y.; Huang, K.-C.; Vittal, R.; Ho, K.-C. CoS Supersedes Pt as Efficient Electrocatalyst for Triiodide Reduction in Dye-Sensitized Solar Cells. *ACS Nano* **2012**, *6*, 7016−7025.

(7) Bao, S.-J.; Li, C. M.; Guo, C.-X.; Qiao, Y. Biomolecule-Assisted Synthesis of Cobalt Sulfide Nanowires for Application in Super-capacitors. *J. Power Sources* **2008**, *180*, 676−681.

(8) Justin, P.; Ranga Rao, G. CoS Spheres for High-Rate Electrochemical Capacitive Energy Storage Application. *Int. J. Hydrogen Energy* **2010**, *35*, 9709−9715.

(9) Yang, Z.; Chen, C.-Y.; Chang, H.-T. Supercapacitors Incorporating Hollow Cobalt Sulfide Hexagonal Nanosheets. *J. Power Sources* **2011**, *196*, 7874−7877.

(10) Huang, G.; Chen, T.; Wang, Z.; Chang, K.; Chen, W. Synthesis and Electrochemical Performances of Cobalt Sulfides/Graphene Nanocomposite as Anode Material of Li-Ion Battery. *J. Power Sources* **2013**, *235*, 122−128.

(11) Wang, Q.; Jiao, L.; Han, Y.; Du, H.; Peng, W.; Huan, Q.; Song, D.; Si, Y.; Wang, Y.; Yuan, H. CoS2 Hollow Spheres: Fabrication and Their Application in Lithium-Ion Batteries. *J. Phys. Chem. C* **2011**, *115*, 8300−8304.

(12) Wang, Y.; Wu, J.; Tang, Y.; Lü, X.; Yang, C.; Qin, M.; Huang, F.; Li, X.; Zhang, X. Phase-Controlled Synthesis of Cobalt Sulfides for Lithium Ion Batteries. *ACS Appl. Mater. Interfaces* **2012**, *4*, 4246−4250.

(13) Wang, J.; Ng, S. H.; Wang, G. X.; Chen, J.; Zhao, L.; Chen, Y.; Liu, H. K. Synthesis and Characterization of Nanosize Cobalt Sulfide for Rechargeable Lithium Batteries. *J. Power Sources* **2006**, *159*, 287−290.

(14) Wu, C.; Jiang, Y.; Kopold, P.; van Aken, P. A.; Maier, J.; Yu, Y. Peapod-Like Carbon-Encapsulated Cobalt Chalcogenide Nanowires as Cycle-Stable and High-Rate Materials for Sodium-Ion Anodes. *Adv. Mater.* **2016**, *28*, 7276−7283.

(15) Matsuzaki, R.; Yajima, A.; Eguchi, M.; Saeki, Y. The Formation Process of Cobalt Sulfide from Tricobalt Tetraoxide Using Sulfur Dioxide as a Sulfidizing Agent. *Bull. Chem. Soc. Jpn.* **1982**, *55*, 1480−1483.

(16) Zhan, J. H.; Xie, Y.; Yang, X. G.; Zhang, W. X.; Qian, Y. T. Hydrazine-Assisted Low-Temperature Hydrothermal Preparation of Nanocrystalline Jaipurite. *J. Solid State Chem.* **1999**, *146*, 36−38.

(17) McDowell, M. T.; Lee, S. W.; Harris, J. T.; Korgel, B. A.; Wang, C.; Nix, W. D.; Cui, Y. In Situ TEM of Two-Phase Lithiation of Amorphous Silicon Nanospheres. *Nano Lett.* **2013**, *13*, 758−764.

(18) Ko, Y. N.; Choi, S. H.; Kang, Y. C. Hollow Cobalt Selenide Microspheres: Synthesis and Application as Anode Materials for Na-Ion Batteries. *ACS Appl. Mater. Interfaces* **2016**, *8*, 6449−6456.

(19) Claridge, S. A.; Castleman, A. W.; Khanna, S. N.; Murray, C. B.; Sen, A.; Weiss, P. S. Cluster-Assembled Materials. *ACS Nano* **2009**, *3*, 244−255.

(20) Pinkard, A.; Champsaur, A. M.; Roy, X. Molecular Clusters: Nanoscale Building Blocks for Solid-State Materials. *Acc. Chem. Res.* **2018**, *51*, 919−929.

(21) Brenna, J. G.; Siegrist, T.; Stuczynski, S. M.; Steigerwald, M. L. The Transition From Molecules to Solids: Molecular Syntheses of $Ni_9Te_6(PEt_3)_8$, $Ni_{20}Te_{18}(PEt_3)_{12}$ and NiTe. *J. Am. Chem. Soc.* **1989**, *111*, 9240−9241.

(22) Stuczynski, S. M.; Kwon, Y. U.; Steigerwald, M. L. The Use of Phosphine Chalcogenides in the Preparation of Cobalt Chalcogenides. *J. Organomet. Chem.* **1993**, *449*, 167−172.

(23) Kolesov, V. A.; Fuentes-Hernandez, C.; Chou, W.-F.; Aizawa, N.; Larrain, F. A.; Wang, M.; Perrotta, A.; Choi, S.; Graham, S.; Bazan, G. C.; Nguyen, T.-Q.; Marder, S. R.; Kippelen, B. Solution-based Electrical Doping of Semiconducting Polymer Films over a Limited Depth. *Nat. Mater.* **2017**, *16*, 474−480.

(24) Kippelen, S.; Endo, K.; Kasuga, K.; Suzuki, M.; Chiba, T.; Pu, Y.-J.; Kido, J. Post-Treatment-Free Solution-Processed Reduced Phosphomolybdic Acid Containing Molybdenum Oxide Units for Efficient Hole-Injection Layers in Organic Light-Emitting Devices. *Inorg. Chem.* **2018**, *57*, 1950−1957.

(25) Jung, D.; Saleh, L. M. A.; Berkson, Z. J.; El-Kady, M. F.; Hwang, J. Y.; Mohamed, N.; Wixtrom, A. I.; Titarenko, E.; Shao, Y.; McCarthy, K.; Guo, J.; Martini, I. B.; Kraemer, S.; Wegener, E. C.; Saint-Cricq, P.; Ruehle, B.; Langeslay, R. R.; Delferro, M.; Brosmer, J. L.; Hendon, C. H.; Gallagher-Jones, M.; Rodriguez, J.; Chapman, K. W.; Miller, J. T.; Duan, X.; Kaner, R. B.; Zink, J. I.; Chmelka, B. F.; Spokoyny, A. M. A Molecular Cross-linking Approach for Hybrid Metal Oxides. *Nat. Mater.* **2018**, *17*, 341−348.

(26) Champsaur, A. M.; Hochuli, T. J.; Paley, D. W.; Nuckolls, C.; Steigerwald, M. L. Superatom Fusion and the Nature of Quantum Confinement. *Nano Lett.* **2018**, *18*, 4564−4569.

(27) Sing, K. S. W.; Everett, D. H.; Haul, R. A. W.; Moscou, L.; Pierotti, R. A.; Rouquerol, P.; Siemieniewska, T. *Pure Appl. Chem.* **1985**, *57*, 603−619.

(28) Egami, T.; Billinge, S. J. L. *Underneath the Bragg Peaks: Structural Analysis of Complex Materials*, 2nd ed.; Elsevier: Amsterdam, 2012.

(29) Bergerhoff, G.; Hundt, R.; Sievers, R.; Brown, I. D. The Inorganic Crystal Structure Data Base. *J. Chem. Inf. Comput. Sci.* **1983**, *23*, 66.

(30) García-García, F. J.; Larsson, A. K.; Norèn, L.; Withers, R. L. The crystal structures of Co3Se4 and Co7Se8. *Solid State Sci.* **2004**, *6*, 725.

(31) Billinge, S. J. L. Nanoscale structural order from the atomic pair distribution function (PDF): There's plenty of room in the middle. *J. Solid State Chem.* **2008**, *181*, 1695.

(32) Billinge, S. J. L.; Kanatzidis, M. G. Beyond crystallography: the study of disorder, nanocrystallinity and crystallographically challenged materials with pair distribution functions. *Chem. Commun.* **2004**, *7*, 749.

(33) Chupas, P. J.; Qiu, X.; Hanson, J. C.; Lee, P. L.; Grey, C. P.; Billinge, S. J. L. Rapid-acquisition pair distribution function (RA-PDF) analysis. *J. Appl. Crystallogr.* **2003**, *36*, 1342.

(34) Proffen, T.; Billinge, S. J. L. PDFFIT, a program for full profile structural refinement of the atomic pair distribution function. *J. Appl. Crystallogr.* **1999**, *32*, 572.

(35) Farrow, C. L.; Juhas, P.; Liu, J. W.; Bryndin, D.; Božin, E. S.; Bloch, J.; Proffen, T.; Billinge, S. J. L. PDFfit2 and PDFgui: computer programs for studying nanostructure in crystals. *J. Phys.: Condens. Matter* **2007**, *19*, 335219.

(36) Juhás, P.; Davis, T.; Farrow, C. L.; Billinge, S. J. L. PDFgetX3: a rapid and highly automatable program for processing powder diffraction data into total scattering pair distribution functions. *J. Appl. Crystallogr.* **2013**, *46*, 560.

(37) Yang, X.; Juhas, P.; Farrow, C. L.; Billinge, S. J. L. xPDFsuite: An End-To-End Software Solution for High Throughput Pair Distribution Function Transformation, Visualization and Analysis. **2014**, arXiv:1402.3163.

(38) Farrow, C. L.; Billinge, S. J. L. Relationship between the atomic pair distribution function and small-angle scattering: implications for modeling of nanoparticles. *Acta Crystallogr., Sect. A: Found. Crystallogr.* **2009**, *65*, 232.

(39) Juhás, P.; Farrow, C. L.; Yang, X.; Knox, K. R.; Billinge, S. J. L. Complex modeling: a strategy and software program for combining multiple information sources to solve ill posed structure and nanostructure inverse problems. *Acta Crystallogr., Sect. A: Found. Adv.* **2015**, *71*, 562.

(40) Jeong, I.-K.; Proffen, T.; Mohiuddin-Jacobs, F.; Billinge, S. J. L. Measuring correlated atomic motion using X-ray diffraction. *J. Phys. Chem. A* **1999**, *103*, 921−924.

(41) Hwang, J.-Y.; Myung, S.-T.; Sun, Y.-K. Sodium-Ion Batteries: Present and Future. *Chem. Soc. Rev.* **2017**, *46*, 3529−3614.

(42) Yabuuchi, N.; Kubota, K.; Dahbi, M.; Komaba, S. Research Development on Sodium-Ion Batteries. *Chem. Rev.* **2014**, *114*, 11636−11682.

(43) Stevens, D. A.; Dahn, J. R. High Capacity Anode Materials for Rechargeable Sodium-Ion Batteries. *J. Electrochem. Soc.* **2000**, *147*, 1271−1273.

(44) Sun, Y.; Zhao, L.; Pan, H.; Lu, X.; Gu, L.; Hu, Y.; Li, H.; Armand, M.; Ikuhara, Y.; Chen, L.; Huang, X. Direct Atomic-Scale Confirmation of Three-Phase Storage Mechanism in $Li_4Ti_5O_{12}$ Anodes for Room-Temperature Sodium-Ion Batteries. *Nat. Commun.* **2013**, *4*, 1870.

(45) Wang, Y.; Yu, X.; Xu, S.; Bai, J.; Xiao, R.; Hu, Y.; Li, H.; Yang, X.; Chen, L.; Huang, X. A Zero-Strain Layered Metal Oxide as the Negative Electrode for Long-Life Sodium-Ion Batteries. *Nat. Commun.* **2013**, *4*, 2365.

(46) Hu, Z.; Wang, L.; Zhang, K.; Wang, J.; Cheng, F.; Tao, Z.; Chen, J. MoS2Nanoflowers with Expanded Interlayers as High-Performance Anodes for Sodium-Ion Batteries. *Angew. Chem., Int. Ed.* **2014**, *53*, 12794−12798.

(47) Fang, Y.; Yu, X.-Y.; Lou, X. W. D. Formation of Hierarchical Cu-Doped CoSe2 Microboxes via Sequential Ion Exchange for High-Performance Sodium-Ion Batteries. *Adv. Mater.* **2018**, *30*, 1706668.

(48) Ding, Y.-L.; Kopold, P.; Hahn, K.; van Aken, P. A.; Maier, J.; Yu, Y. A Lamellar Hybrid Assembled from Metal Disulfide Nanowall Arrays Anchored on a Carbon Layer: In Situ Hybridization and Improved Sodium Storage. *Adv. Mater.* **2016**, *28*, 7774−7782.